THE ASTROPHYSICAL JOURNAL, 385:265–272, 1992 January 20

THE MULTIPLE MOLECULAR WINDS OF CRL 2688

K. YOUNG,[1] G. SERABYN,[2] T. G. PHILLIPS,[2] G. R. KNAPP,[3] R. GÜSTEN,[4] AND A. SCHULZ[4]

Received 1991 May 28; accepted 1991 August 1

ABSTRACT

Three rotational transitions of $^{12}C^{16}O$, two of $^{13}C^{16}O$, and one of $^{1}H^{12}C^{14}N$ were observed toward the proto–planetary nebula CRL 2688. The spectra reveal a previously undetected wing of emission representing an outflow velocity of about 100 km s^{-1}. The mechanical momentum in this wind appears to be too large to be supplied by radiation pressure. Also observed is an absorption feature which is on the blueshifted side of the spectrum with respect to the systemic velocity. This feature is interpreted as due to the low-velocity wind absorbing radiation from higher velocity gas near the star. High-resolution spectra of this absorption feature show that its blue edge is very sharp, providing a tight constraint on the turbulent velocity of the low-velocity stellar wind.

Subject headings: ISM: individual (CRL 2688) — stars: evolution — stars: mass-loss — stars: post–asymptotic giant branch (post–AGB)

1. INTRODUCTION

CRL 2688, the Egg nebula, is believed to be a proto–planetary nebula (PPN) (Rodríguez 1987), nearing the end of the copious mass-loss phase which terminates the asymptotic giant branch (AGB) phase of evolution. Most of the mass lost during the AGB stage is ejected at a low velocity, typically 15 km s^{-1}. This low-velocity wind is probably driven by radiation pressure on dust, which can condense in the atmosphere of a cool red giant star (see a review by Olofsson 1988). Optically, CRL 2688 is a highly polarized double-lobed nebula. These optical lobes scatter the light from the central star and reveal that the star's spectral type is F5 1a, with some anomalous features arising from short carbon-chain molecules (Crampton, Cowley, & Humphreys 1975). Between these two optical lobes is a small infrared source with a temperature of 150 K (Ney et al. 1975). This infrared source is extended, and its position and orientation suggest that it is a torus of dust surrounding the hidden star. The fact that both of the optical lobes are visible suggests that we must be nearly in the plane of the torus. CRL 618, another probable PPN, has an even hotter photosphere with a spectral type of B0 (Westbrook et al. 1975). These elevated temperatures show that both of these objects have moved off the AGB and are in the process of uncovering their white dwarf cores. Since it is unlikely that grains can continue to condense in such hot atmospheres, the mechanism by which the final portion of the extended atmosphere is expelled probably differs from the mechanism operating on the AGB. Evidence is accumulating that the material expelled by PPNs is ejected at a much higher velocity than the material lost while the star was on the AGB. H_2 emission at an outflow velocity of 125 km s^{-1} has been detected surrounding CRL 618 (Burton & Geballe 1986), as well as CO emission with a velocity in excess of 190 km s^{-1} (Gammie et al. 1989; Cernicharo et al. 1990).

Another interesting feature of CRL 2688's molecular spectra is the presence of a deep absorption dip (Smith et al. 1990; Kawabe et al. 1987). This feature is probably caused by the low-velocity wind absorbing radiation from the high-velocity material closer to the star. We have obtained high-velocity resolution spectra of this absorption feature which show that it has a very steep blue edge which is smeared out in low resolution spectra. The shape of this absorption feature allows the amount of turbulence in the expanding envelope to be calculated. This quantity is an important input parameter to radiative transfer models of CRL 2688 because it determines the local line width of a volume element in the envelope. If this line width is much less than 1 km s^{-1}, infrared pumping of the rotational-vibrational lines is hindered by large optical depths in the infrared lines along the radial direction (Morris & Alcock 1977). The amount of turbulence in the envelope can also constrain models of the innermost regions of the envelope, where the bipolar morphology probably arises. Morris (1981) proposed that the bipolar morphology of CRL 2688 was the result of an interacting binary system. The orbital motions of a close binary might increase the turbulence in the molecular outflow above the value found in the envelope of an isolated red giant star. Finally, the corotation of the molecular envelope with the central star, which was proposed by Bieging & Nguyen-Quang-Rieu (1988), could affect the shape of this absorption feature.

2. OBSERVATIONS

All observations presented here were made at the Caltech Submillimeter Observatory[5] (CSO) on Mauna Kea, Hawaii. The $^{12}CO(2–1)$ line was observed in 1989 June (Figs. 1*a* and 3*a*) with an SIS receiver (Ellison & Miller 1987), having a double-sideband temperature of about 100 K. Two 1024 channel AOS backends were used, one having a total bandwidth of 500 MHz, and the other having a total bandwidth of 50 MHz. The $^{12}CO(3–2)$ transition was observed (Figs. 1*b*, 2*a*, and 3*b*) with an SIS receiver (Ellison et al. 1989), having a double-sideband temperature of about 200 K. Once again two backends were used; the 500 MHz in 1989 May, and the 50 MHz in 1990 June. A spectrum of the $^{12}CO(4–3)$ transition was obtained in 1990 October (Fig. 1*c*), using a Schottky diode receiver built by the

[1] 405-47, California Institute of Technology, Pasadena, CA 91125.
[2] 320-47, California Institute of Technology, Pasadena, CA 91125.
[3] Department of Astrophysical Sciences, Princeton University, Princeton, NJ 08544.
[4] MPI für Radioastronomie, Auf dem Hügel 69, D-5300 Bonn 1, Germany.

[5] The CSO is operated by the California Institute of Technology under funding from the National Science Foundation, contract AST-9015755.

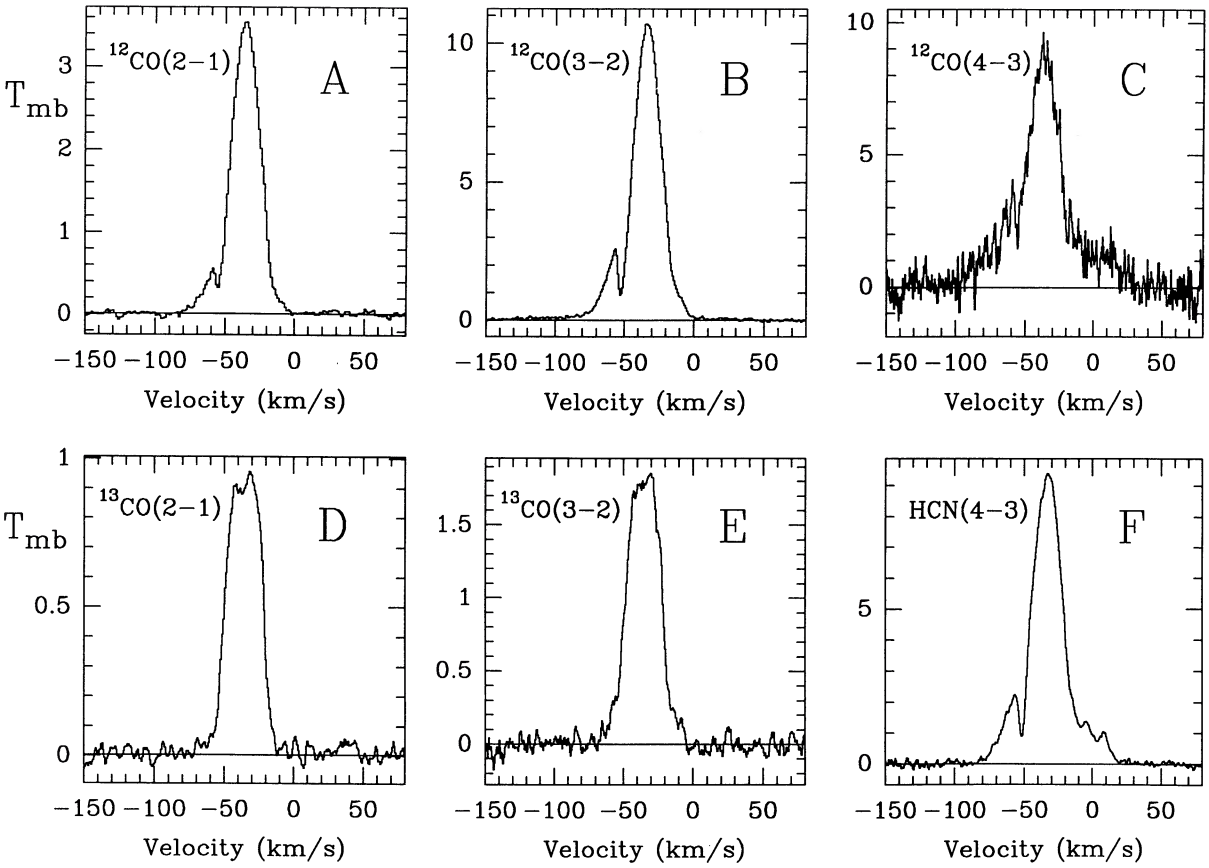

FIG. 1.—Spectra for five molecular transitions of CO and one of HCN. The wide wing can be seen in the ^{12}CO(4–3) and ^{12}CO(3–2) spectra. In Fig. 2 it is shown with an expanded temperature scale. The self-absorption feature, at -55 km s^{-1} is visible in all three ^{13}CO spectra, but neither ^{13}CO spectrum. Fig. 3 shows this feature with higher spectral resolution.

Max-Planck-Institut für Radioastronomie (Keen et al. 1986) with a double-sideband temperature of 1150 K, and the 500 MHz backend. Finally, spectra of the ^{13}CO(2–1), ^{13}CO(3– 2), and HCN(4–3) transitions were taken in April of 1991 using the same SIS receivers, and the 500 MHz AOS. Tables 1 and 2 give the details of these integrations.

The coordinates used for CRL 2688 were $\alpha_{1950} = 21^h00^m20^s.0$, $\delta_{1950} = 36°29^m44^s.0$ for all observations except for those of the CO(4–3) transition, where $\alpha_{1950} = 21^h00^m19^s.7$, $\delta_{1950} = 36°29^m45^s.0$ was used. For the five lower frequency lines, the pointing was checked and adjusted by taking test scans in a five-point cross centered on the source. For the CO(4–3) spectrum, Mars was used as the pointing reference. Scans were taken while position-switching at 0.05 Hz between the source and two off-source positions located 3′ away in azimuth, on either side of the source.

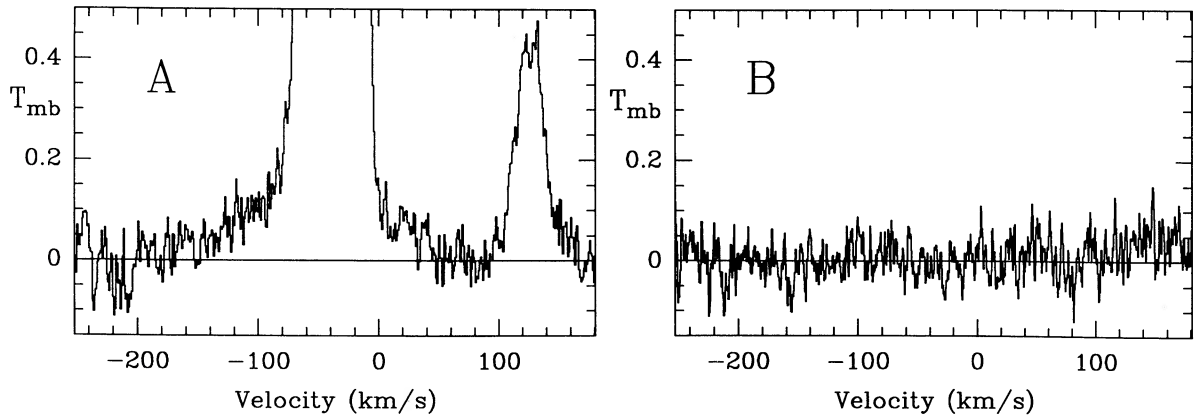

FIG. 2.—(*a*) Weak high-velocity emission in the ^{12}CO(3–2) spectrum from Fig. 1*b* is shown with an expanded vertical scale. The high-velocity emission extends from about -160 to 50 km s^{-1}. The line at 125 km s^{-1} is HC_3N(38–37). (*b*) Sum of 16 scans taken at a position 20′ away from the source, in order to check the baseline stability. These scans were interleaved in time with the on-source scans which were summed to produce plot A.

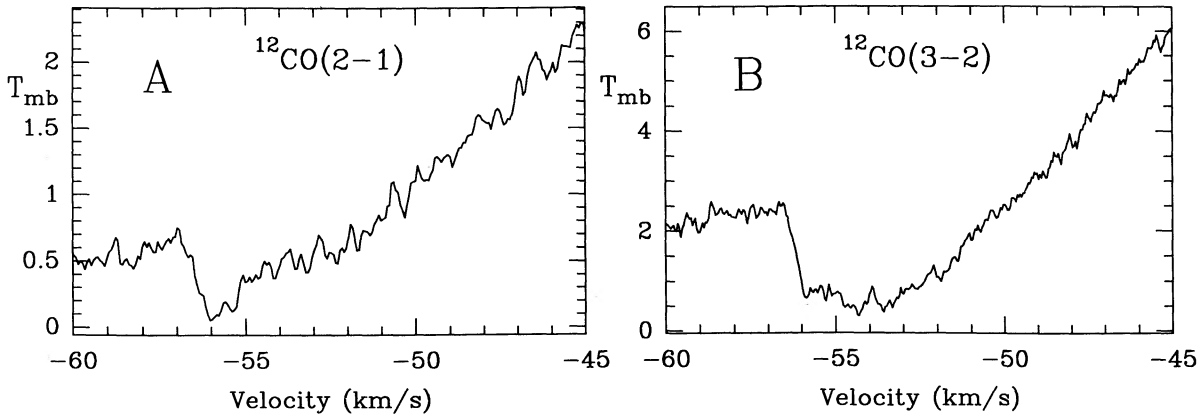

FIG. 3.—(*a*) The self-absorption dip in the ^{12}CO(2–1) transition. (*b*) The self-absorption dip in the ^{12}CO(3–2) transition. The blue edge of this feature has a width of only 0.5 km s^{-1}.

When viewed on an expanded temperature scale, the CO(3–2) spectrum shows a low-intensity feature between LSR velocities −160 and 40 km s^{-1} (Fig. 2*a*). A broad, weak feature like this might arise from instrumental imperfections, so the 18 scans making up this spectrum were interleaved with scans taken 20′ away from the source. The combined off-source scans (Fig. 2*b*) show that the AOS baseline was flat over the region in question at the time of the observations. Even though the off-source scans were flat, the high-velocity wings in the on-source scans could still be spurious, if an instrumental defect existed which produced broad wings around any strong line. To eliminate this possibility, a CO(3–2) profile of CIT 6, with signal-to-noise ratio comparable to Figure 1*b*, was obtained. No broad wings appeared in the CIT spectrum. It is therefore very unlikely that the broad wings shown in Figure 2*a* arose from an instrumental defect.

The spectra were calibrated by placing an absorber at a temperature of 280 K into the telescope's beam. Linear baselines were fitted to the regions of the 500 MHz spectra judged free of emission and were subtracted from the data. No baselines were removed from the 50 MHz spectra, because there was no region free of emission. Finally the spectra were corrected for the coupling of the receiver to the telescope by dividing them by the telescope's main beam efficiency, which was determined from planetary measurements. All temperatures presented here are therefore on the main beam brightness scale (T_{mb}).

TABLE 2

HYPERFINE LEVELS OF THE HCN(4–3) SEXTET

Transition	Frequency (GHz)	Relative Strength-(km s^{-1})	Velocity Shift
$F = 5 \rightarrow 4$.....	354.505518	0.4074	0.039
$F = 4 \rightarrow 4$.....	354.503861	0.0208	−1.364
$F = 4 \rightarrow 3$.....	354.505472	0.3125	0.000
$F = 3 \rightarrow 4$.....	354.505837	0.0003	0.309
$F = 3 \rightarrow 3$.....	354.507449	0.0208	1.673
$F = 3 \rightarrow 2$.....	354.505361	0.2381	−0.094

3. ANALYSIS

The ^{12}CO(3–2) spectrum (Figs. 1*b* and 2*a*) has the highest signal-to-noise ratio of the three transitions observed. In it can be seen three velocity components. The first, a low-velocity wind (LVW), has a very nearly parabolic profile characteristic of unresolved, optically thick emission. It is centered at −33.3 km s^{-1}, and the outflow velocity is 18.0 km s^{-1}. The peak main beam temperature for the ^{12}CO(3–2) and ^{12}CO(4–3) transitions, 10.8 and 9.1 K respectively, are similar. However, the ^{12}CO(2–1) peak temperature is only 3.4 K. These values suggest that the region where the LVW feature arises is resolved by the ^{12}CO(3–2) and ^{12}CO(4–3) beams, but not by the ^{12}CO(2–1) beam. The profiles of the LVW in both the ^{13}CO(2–1) and ^{13}CO(3–2) spectra are flat-topped indicating

TABLE 1

CRL 2688 OBSERVATIONS

Figure	Transition	Frequency (GHz)	Resolution	Main Beam Efficiency	Velocity Resolution (km s^{-1})	T_{sys} SSB (K)	Integration Time (minutes)	RMS Noise (mK)
1*a*	^{12}CO(2–1)	230.538	32″	0.72	1.3	520	26	20
1*b*	^{12}CO(3–2)	345.796	21	0.60	0.85	570	22	19
1*c*	^{12}CO(4–3)	461.041	15	0.50	0.64	9000	21	390
1*d*	^{13}CO(2–1)	220.399	33	0.72	1.3	755	25	15
1*e*	^{13}CO(3–2)	330.588	22	0.60	0.89	1800	28	26
1*f*	HCN(4–3)	354.505[a]	20	0.60	0.83	1400	19	45
3*a*	^{12}CO(2–1)	230.538	32	0.72	0.20	440	33	53
3*b*	^{12}CO(3–2)	345.796	21	0.60	0.13	430	23	62

[a] The frequency given here is the strength weighted average of the six hyperfine levels which make up the HCN(4–3) transition. The frequencies of the individual levels are given in Table 2. They were calculated using spectral constants measured by DeLucia & Gordy (1969).

that the envelope is optically thin in these transitions (Morris 1980). Comparison of the temperatures of the main and isotopically substituted lines at the systemic velocity allows the optical depth of the LVW to be calculated. Assuming a $^{12}CO/^{13}CO$ ratio of 20 (Wannier & Sahai 1987; Sopka et al. 1989), the optical depth of the LVW is 4.0 in $^{12}CO(3–2)$ and 6.6 in $^{12}CO(2–1)$.

The second component, a moderate velocity wind (MVW) cuts off at a velocity of -73 km s^{-1} on the blue edge of the $^{12}CO(3–2)$ transition, giving an outflow velocity of ~ 40 km s^{-1}. The red wing of the MVW is weaker than the blue wing in all transitions and falls to zero intensity at -2 km s^{-1} in the $^{12}CO(3–2)$ spectrum. The blue wing of the HCN(4–3) profile's MVW resembles that of $^{12}CO(3–2)$ very closely, while its red wing, which shows two small peaks not seen in any of the CO spectra, extends to 28 km s^{-1} and resembles the red wing seen in the CO(4–3) profile. Although the HCN(4–3) transition has six components due to hyperfine structure, the frequency difference between the highest and lowest frequency components corresponds to a velocity difference of only 3 km s^{-1}. Therefore the hyperfine structure cannot be responsible for much of the 100 km s^{-1} width of the HCN profile. The "peak" main beam temperature of the MVW feature, measured at -57 km s^{-1} (just to the left of the self-absorption dip), is 0.6, 2.6, and 3.6 for the $^{12}CO(2–1)$, $^{12}CO(3–2)$, and $^{12}CO(4–3)$ transitions. The ratios of the peak MVW temperature to that of the LVW are 0.16, 0.24, and 0.40 for the three transitions. This increase in the relative strength of the MVW as the telescope's beam shrinks indicates that the MVW arises from a smaller region than the LVW and is probably not resolved by either the $^{12}CO(2–1)$ or $^{12}CO(3–2)$ beams. The MVW is clearly visible in the $^{13}CO(3–2)$ spectrum, and its blue wing is marginally detected in the $^{13}CO(2–1)$ spectrum. The MVW's $^{13}CO(3–2)$ profile appears to cover a smaller velocity range than its $^{12}CO(3–2)$ profile, suggesting that the optical depth of both transitions decreases as the velocity extrema are approached. Comparison of the main beam temperatures of ^{12}CO and ^{13}CO at -57 km s^{-1} yields a maximum MVW optical depth of 2.1 for $^{12}CO(2–1)$ and 2.3 for $^{12}CO(3–2)$, once again using $^{12}CO/^{13}CO = 20$.

Finally, on an expanded scale Figure 2*a* shows a third component, a high-velocity wind (HVW) in the $^{12}CO(3–2)$ profile. The HVW extends over a velocity range of -160 ± 20 to 40 ± 10 km s^{-1}, which implies the outflow velocity of this material is 100 ± 10 km s^{-1}. The shape of the HVW profile is triangular, as is that of the HVW surrounding CRL 618 (Gammie et al. 1989; Cernicharo et al. 1990), suggesting that the same acceleration mechanism may be at work in both cases. This shape is not apt to arise from a spherical envelope of gas expanding at a constant velocity (cf. Morris, Lucas, & Omont 1985).

The $^{12}CO(2–1)$ spectrum shows the LVW and MVW clearly, but not the HVW. The $^{12}CO(4–3)$ and HCN(4–3) spectra show emission with a total extent intermediate between the extents of the MVW and the HVW, with an outflow velocity of at least 60 km s^{-1}.

Figure 3 shows CRL 2688's absorption feature, with the increased velocity resolution provided by the 50 MHz AOS. The depth of the absorption feature in the $^{12}CO(2–1)$ transition (Fig. 3*a*) is much greater than it appears in the low-resolution spectrum (Fig. 1*a*), and at a velocity of -56.0 km s^{-1} T_{mb} drops nearly to 0. Both the $^{12}CO(2–1)$ and $^{12}CO(3–2)$ absorption features (the latter shown in Fig. 3*b*) have very steep blue edges. The edge of the $^{12}CO(3–2)$ feature is only 0.5 km s^{-1} wide. The frequency resolution of the 50 MHz AOS was measured by examining a calibration oscillator, which produced a peak with a full width at half-maximum corresponding to 0.13 km s^{-1} at the frequency of $^{12}CO(3–2)$.

4. A MODEL FOR THE ABSORPTION FEATURE

The absorption feature probably arises when radiation from the MVW is absorbed by the LVW, since it lies at the cutoff velocity of the LVW's profile. The absorbing LVW gas must be situated between the observer and the MVW, since absorption is only seen on the blueshifted side of the line. A simple model that could give rise to this feature is shown in Figure 4(i). In this model the MVW and LVW arise in separate, concentric spherical regions.

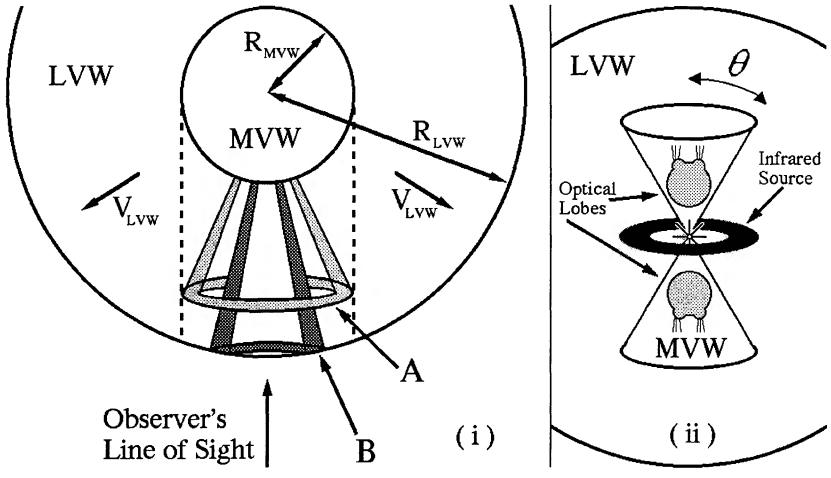

FIG. 4.—(i) The model for the absorption feature is shown. Broad line emission from the MVW region is absorbed by the surrounding LVW region. The LVW is assumed to be expanding at a constant velocity, so all material within a cone with axis of symmetry along the observer's line of sight has the same radial velocity. Cone A is an example of a cone containing material with a radial velocity less than V_c (see eq. [1]). Cones of this type are truncated by a cylinder of radius R_{MVW}. Material in cone B had a radial velocity greater than V_c. Such cones are truncated when they reach the edge of the LVW envelope. (ii) Here an alternative geometry is shown, with the MVW gas occupying two conical regions, rather than a complete sphere as in (i). The conic axes are assumed to coincide with the axis defined by the optical nebula. θ measures the opening angle of the cones, relative to this axis. Fig. 4(i) corresponds to the case $\theta = 90°$. If the observer is located in the equatorial plane of the object, then $dm(v)/dv$ has the form of eqs. (2a)–(2c), regardless of the value of θ.

The material in the inner MVW region emits radiation which can be absorbed by the outer LVW envelope. If the thermal and turbulent velocities are small when compared to V_{LVW}, then all the material within a truncated cone, such as either of the ones shown in Figure 4(i), will have the same radial velocity. If the MVW region is unresolved by the telescope, then all the material within the cone contributes to the absorption seen at the central position. Let v be the radial velocity offset from CRL 2688's LSR velocity. If the partition of CO among the low-J states is the same at all positions where LVW gas is present, the depth of the absorption feature at a given velocity v will be determined by the mass present within the cone with that radial velocity. The absorbing cones fall into two categories. Cones with small $|v|$ (e.g. cone A in Fig. 4[i]) all have a base radius equal to the radius of the MVW region (R_{MVW}). Cones with $|v| \approx V_{LVW}$ (e.g., cone B) will have smaller base radii, because they will be truncated at the outer radius of the LVW (R_{LVW}). The value of v at which the transition between these two regimes occurs is

$$V_c = V_{LVW}\sqrt{1 - \left(\frac{R_{MVW}}{R_{LVW}}\right)^2}. \quad (1)$$

Let us assume that during the period when the LVW was formed, CRL 2688 was expelling material at a constant rate. The density of CO will then fall off as $1/r^2$. If the outer radius of the MVW is also the inner radius of the LVW, and if ρ_0 is the density of CO at that radius, then $\rho_0 R_{MVW}^2/r^2$ is the density at radius r within the LVW region. All radiation in a velocity interval of width dv centered at v will be absorbed by material of mass $dm(v)$ given by

$$\frac{dm(v)}{dv} = 0 \quad \text{for } 0 < v \text{ and for } v < -V_{LVW} \quad (2a)$$

$$\frac{dm(v)}{dv} = \frac{2\pi\rho_0 R_{MVW}^3}{V_{LVW}}\left(\frac{1}{[1-(v/V_{LVW})^2]^{1/2}} - 1\right) \quad \text{for } -V_c \le v \le 0 \quad (2b)$$

$$\frac{dm(v)}{dv} = \frac{2\pi\rho_0 R_{MVW}^2(R_{LVW} - R_{MVW})}{V_{LVW}} \quad \text{for } -V_{LVW} \le v < -V_c. \quad (2c)$$

Equation (2c) is constant for all values of v. Because of this the absorption feature has a width comparable to the velocity range over which equation (2c) holds. This range of velocities is itself determined by V_c, which is a function of R_{MVW}/R_{LVW}. Therefore the width of the absorption feature allows the relative sizes of the MVW and LVW regions to be determined, even if neither one can be resolved by the telescope.

In order to compare this model with the observations in Figure 3*b*, a model of the emission being absorbed is needed. The profile of the emission from the MVW will be approximated by a Gaussian function centered at the systemic velocity, V_{LSR}. For simplicity, all velocity structure within the MVW will be ignored. The profile of the LVW emission will be assumed to be parabolic. If *line*(v) is a function giving the profile of the line in the absence of absorption, and if we ignore reemission of the absorbed radiation, the profile with absorption is given by

$$\text{profile}(v) = \text{line}(v)\exp\left[C\frac{dm(v)}{dv}\right],$$

where C is a constant.

There is a discontinuity in the equations above for $dm(v)/dv$ at $v = V_{LVW}$. This is the blue edge of the absorption feature. Figure 3*b* shows that the blue edge is very sharp, but not discontinuous. The total width of the blue edge is 0.5 km s^{-1}. This finite width is caused by a combination of instrumental resolution, thermal broadening and turbulent motion within the LVW.

Figure 5 shows the absoprtion model given in equations (2a)–(2c) compared with the 50 MHz AOS data for the ^{12}CO(3–2) line. In order to produce a blue edge with a finite width, the analytic expressions for $dm(v)/dv$ were convolved with a Gaussian function. The model parameters were fitted in a least-squares sense, using Powell's direction set method of minimization (Press et al. 1988). Table 3 lists the parameters and their best fit values. The rms difference between the model and data is 0.18 K.

Taking the frequency resolution of the 50 MHz AOS into account, the Gaussian broadening of the best fit model is 0.56 km s^{-1}. If all of this broadening were due to the LVW's thermal velocity, the implied temperature would be 190 K. Since CRL 2688's central infrared source has a temperature of only 150 K (Ney et al. 1975), it is very unlikely that the gas temperature could be so high. Truong-Bach et al. (1990) obtained a value of $\sim$15 K for the temperature of the outer envelope by solving the radiative transfer problem using the

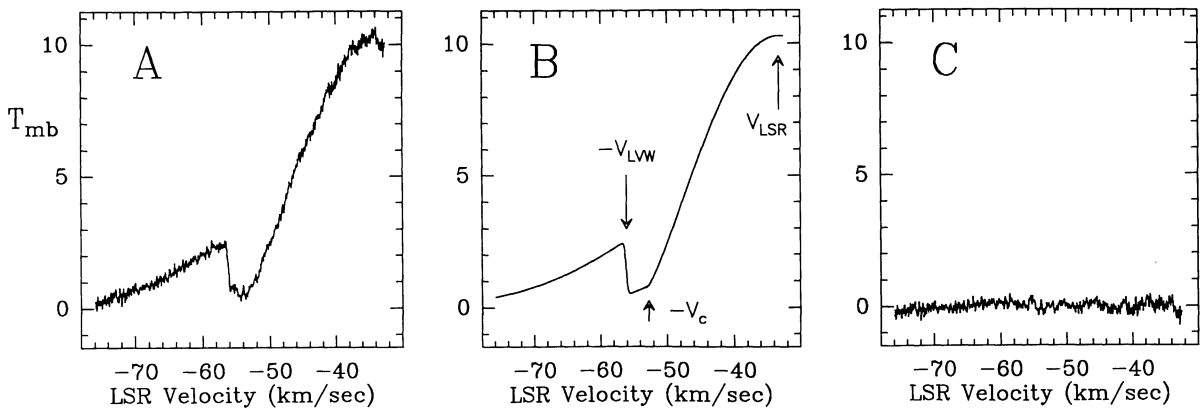

FIG. 5.—(*a*) The full 50 MHz ^{12}CO(3–2) spectrum. (*b*) The model spectrum using the best-fit parameters. (*c*) The residuals: A − B.

TABLE 3

BEST-FIT PARAMETERS FOR ABSORPTION FEATURE MODEL

Parameter Number	Description	Best-Fit Value
1	Maximum optical depth of absorption line	1.7
2	R_{MVW}/R_{LVW}	0.52
3	V_{LVW}	22.8 km s^{-1}
4	Peak T_{mb} from LVW emission	4.9 K
5	Full width at half-maximum of MVW profile	44.0 km s^{-1}
6	Peak T_{mb} from MVW emission	5.3 K
7	V_{LSR} of CRL 2688	−33.3 km s^{-1}
8	Full width at half-maximum of convolved Gaussian	0.58 km s^{-1}

large velocity gradient approximation. If the temperature of the LVW region is ~15 K, then most of the broadening must be due to large scale turbulent motion.

5. DISCUSSION

5.1. *The High-Velocity Wind*

The fast wind in CRL 618 seen in the ^{12}CO(3–2) transition (Gammie et al. 1989) has a velocity of ~190 km s^{-1}, about twice the value of the HVW from CRL 2688. The map of the HVW from CRL 618 made by Cernicharo et al. shows that the HVW is bipolar and slightly tilted along the line of sight. If the HVW surrounding CRL 2688 is also bipolar, then some of the difference between the expansion velocities may be due to differing angles of inclination of the outflows with respect to our line of sight. The optical nebulosities of both these objects have a bipolar morphology. If the bipolar axes of the optical nebulae and HVWs agree, then the deprojected velocities of the HVWs can be calculated. An emission-line study of the CRL 618 nebula gave an inclination of 45° (Carsenty & Solf 1982). Monte Carlo simulations of scattering by dust in the reflection nebula centered on CRL 2688 (Yusef-Zadeh, Morris, & White 1984) yielded an inclination angle of 16° for the equatorial plane. Using these inclinations, the deprojected outflow velocities are 270 km s^{-1} for CRL 618 and 360 km s^{-1} for CRL 2688.

The CO(3–2) spectrum of CRL 618 (Gammie et al. 1989) shows a narrow self-absorption dip at the blueshifted edge of that object's LVW feature, as do the CO(2–1), HCO$^+$(3–2), and HC_3N(25–24) spectra of Cernicharo et al. (1990). These absorption features may arise from the LVW material absorbing radiation from CRL 618's HVW. However, the very deep absorption feature seen in the Cernicharo et al. HCO$^+$(1–0) profile passes below $T_{mb} = 0$ and must arise from absorption by the LVW of CRL 618's underlying continuum emission. Absorption of the continuum could also be responsible for the weaker absorption dips seen in the other molecular transitions. One might expect to see a similar absorption dip at the blue edge of the MVW feature in CRL 2688's CO(3–2) profile. No such feature is seen (see Fig. 2*a*). The lack of such a feature could indicate that the MVW is not situated between the observer and the HVW. A more likely explanation is that the optical depth of the MVW feature at its velocity extrema is too low to produce self-absorption. The latter interpretation is supported by the MVW's optically thin ^{13}CO(3–2) profile, which extends over a smaller velocity range than does the optically thicker ^{12}CO(3–2) profile (see Figs. 1*b* and 1*e*).

The CRL 2688 HVW is considerably less conspicuous than that of CRL 618. In the spectra of Gammie et al. (1990), the ratio of the peak main beam temperature of the CRL 618 HVW to that of its LVW is 0.127, while the ratio for CRL 2688 is 0.018. CRL 618 has already developed an H II region (Kwok & Bignell 1984), but CRL 2688 has not (Spergel, Giuliani, & Knapp 1983). CRL 618's photosphere (spectral type B0) is hotter than that of CRL 2688 (spectral type F5). These facts all suggest that CRL 2688 left the AGB more recently than CRL 618.

Gammie et al. (1990) used the large velocity gradient (LVG) model of Morris (1980) to estimate the mass and size of the HVW from CRL 618. The model assumes spherical symmetry and that both the mass loss rate and outflow velocity are constant. The data presented here showing the HVW from CRL 2688 were modeled using the same LVG code. Table 4 shows the best-fit parameters for both stars. The shape of the HVW profiles, and the relative strengths of the ^{12}CO(3–2) and ^{12}CO(2–1) transitions, suggest that in both cases the HVW is unresolved by the CSO's ^{12}CO(3–2) beam, and therefore have $r \leq 10''$. However the estimates of the radii presented in Table 4 are very poorly constrained.

Knapp et al. (1982) showed that radiation pressure was adequate to explain the mass-loss rates observed in most evolved stars. If a stellar wind is driven by radiation pressure, then the rate of momentum transfer to the wind must be less than or equal to the momentum of the star's radiation

$$\dot{M}V \leq L_*/c\ .$$

For the PPNs CRL 618 and CRL 2688, the momentum in the LVW appears to exceed the momentum available in the radiation field by factor of 7 (Knapp et al. 1982; Knapp 1986). This might be due to a decrease in the brightness of the central star as it leaves the AGB. However, the values of $\dot{M}V_{HVM}$ in Table 3 exceed the value available from radiation pressure by a factor of about 100, even assuming the central stars have the theoreti-

TABLE 4

HIGH-VELOCITY WIND RADIATIVE TRANSFER MODEL RESULTS

Object	Distance (pc)	R_{HVW} (10^{15} cm)	V_{HVW} (km s^{-1})	M ($M_\odot$)	$\dot{M}$ (10^{-4} $M_\odot$ yr^{-1})	$\dot{M}V_{HVW}$ (10^{29} g cm s^{-2})
CRL 618	1300	100	200	0.1	7	9
CRL 2688	1000	5	100	0.016	10	6

cal maximum luminosity for an AGB star, $5 \times 10^4\ L_\odot$ (Iben & Renzini 1983). Therefore it seems unlikely that radiation pressure drives the HVW.

Cernicharo et al. (1990) suggest two possible mechanisms for the acceleration of the HVW from CRL 618. One, originally proposed by Morris (1987), is for acceleration to occur via an interaction with a small orbiting companion star. The second method proposed is that the shock front from the PPN's small H II region accelerates and dissociates the dense material in the LVW. This material then recombines to form molecules, traveling at a high velocity. However the absence of an H II region associated with CRL 2688 shows that the HVW can form in the absence of a high-speed ionized wind. There is currently no clearly favored mechanism for producing the HVW.

5.2. *The Absorption Dip at* -55 km s^{-1} *and the MVW Feature*

The absorption model gives a value of 0.52 for the ratio of the radius of the MVW region to that of the LVW. Truong-Bach et al. (1990) calculated that the CO envelope would be truncated by photodissociation at a radius of 3×10^{17} cm. Using this value as $R_{\rm LVW}$ gives $R_{\rm MVW} = 1.5 \times 10^{17}$ cm. Assuming a distance of 1 kpc (Ney et al. 1975), the angular diameter of the MVW would be 20″. Truong-Bach et al. argue that published detections and nondetections of this feature from a variety of telescopes suggest that the MVW region cannot have a diameter of more than 15″. However one of the observations used by these authors to constrain the size of the MVW region was the nondetection of the absorption dip in the ^{12}CO(2–1) spectrum obtained by Heiligman et al. (1986). Truong-Bach et al. suggest that this nondetection was caused by the large beam of the NRAO 12 m telescope. The ^{12}CO(2–1) profiles presented here, taken with a 10.4 m telescope and a correspondingly bigger beam, clearly show the absorption feature, implying the feature is masked by noise in the Heiligman et al. spectrum.

The Morris LVG code was used to calculate the mass-loss rates for both the MVW and the LVW. It showed that it is not possible to match the observed intensities of the LVW component if all the LVW gas is located further than $R_{\rm MVW}$ from the star. If the LVW gas is confined within $R_{\rm LVW} = 3 \times 10^{17}$ cm and the MVW is confined within $R_{\rm MVW} = 1.5 \times 10^{17}$ cm, then the LVG model which best reproduces the observed line profiles has a total mass loss rate of $1.5 \times 10^{-4}\ M_\odot$ yr^{-1}. This agrees well with the value of $1.7 \times 10^{-4}\ M_\odot$ yr^{-1} found by Truong-Bach et al. (1990). To produce the MVW profile, half of the gas within $R_{\rm MVW}$ must have the MVW velocity. The total mass in the MVW is 0.1 $M_\odot$, and that of the LVW is 0.7 $M_\odot$. Additional evidence that some of the LVW gas must be located inside $R_{\rm MVW}$ is provided by a comparison of the ^{12}CO(3–2) and ^{13}CO(3–2) profiles, which yields an optical depth for the main line of 4.0, while the best-fit model results presented in Table 2 give a maximum optical depth in the absorption feature of only 1.7. Therefore the model shown in Figure 4(i) is at best only an approximation to the true source geometry. If the MVW region is optically thick, two other source geometries would give rise to an absorption feature with an identical shape. The first alternative is that the MVW could arise in a hollow spherical shell, with LVW gas both inside the outside the shell. The second possibility is that the MVW is confined to two conical regions oriented along a symmetry axis perpendicular to our line of sight, as is shown in Figure 4(ii). The morphology of the optical reflection nebula shows that the bipolar outflow does have this orientation. The hollow shell geometry seems less likely, because the HCN(4–3) transition clearly shows the MVW, with the same relative intensity as it is seen in CO(3–2). Since HCN traces high-density gas, some of the MVW gas is probably located very near the star.

The presence of two of the velocity components, the LVW and MVW, could be explained by the binary model proposed by Morris (1987). In this model an accretion disk surrounds both stars. The LVW was expelled from the former red giant star, and the higher velocity material was expelled from the vicinity of the companion star. However, the shape of the blue edge of the absorption feature at -55 km s^{-1} tells us that the LVW has a well-ordered velocity field, with no turbulent motions in excess of ~ 0.5 km s^{-1}. If CRL 2688 is an interacting binary system, it is likely that velocity variations comparable to the orbital velocity of the red giant star would be introduced to the LVW. For an interacting binary, such as envisioned by Morris (1981), velocity variations of at least a few km s^{-1} would be expected in the inner portion of expanding envelope. If the binary ejection model is correct, these variations must have been damped out as the LVW envelope expanded, presumably via collisions. It would be useful to observe the absorption feature in spectral lines arising from material at a higher temperature and/or density than is required to produce CO(3–2) emission. Such observations would probe more deeply into the envelope and might reveal a more turbulent inner region.

Bieging & Nguyen-Quang-Rieu (1988) observed the HCN(1–0) transition with the Hat Creek interferometer. They produced a map of the velocity field of CRL 2688's inner region. The velocity field is dominated by the velocity gradient of 5 km s^{-1} aligned with the bipolar axis. In addition, they report a velocity gradient of 2.4 km s^{-1} along the orthogonal axis. The authors argue that this velocity gradient arises from the rotation of an expanding torus. The derived rotational speed is 1.2 km s^{-1}, at a radius of 5.6×10^{16} cm. If this material conserves angular momentum as it expands, then the velocity gradient across the entire torus should be 0.9 km s^{-1} when the material passes through $R_{\rm MVW}$. However, if the model presented here for the formation of the absorption feature is correct, the LVW material absorbing radiation near the blue edge of the feature is located just outside the $R_{\rm MVW}$. Therefore the rotation of the torus should produce a broader blue edge than is observed.

If the MVW region has expanded at a constant velocity of $V_{\rm MWV} = 43$ km s^{-1}, the size estimate of 1.5×10^{17} cm gives an age for the MVW of $\sim 10^3$ yr. This is similar to the times of 500 and 5000 yr than Schönberner (1983) calculated as the times required for post–AGB stars with masses of 0.8 and 1.0 $M_\odot$, respectively, to reach spectral type F5 ($T_{\rm eff} = 6500$ K). Perhaps the mass-loss process changes as the star leaves the AGB, and this change results in the remainder of the red giant envelope being expelled at a higher velocity. On the other hand, there is no spectral feature similar to that of the MVW in the spectrum of CRL 618, which also left the AGB recently.

6. CONCLUSIONS

The spectra of the post–AGB star CRL 2688 presented here have revealed several new features. A high-velocity wind (HVW) of at least ~ 100 km s^{-1} has been seen, along with the 45 km s^{-1} and 23 km s^{-1} winds which had been detected in earlier studies. In addition, an absorption feature on the blue side of the spectrum has been observed at high spectral resolution and shown to have a distinctive shape. A simple

model has been developed which accurately reproduces the shape of this feature, from which it is deduced that the radius of the MVW is about one-half that of the LVW, and that the turbulent velocity is about 0.5 km s^{-1}. The velocity field is therefore well ordered, providing a constraint for binary models of this object. The shape of the blue edge of the absorption feature also argues against bulk motions exceeding 0.5 km s^{-1} in the expanding envelope, such as would be introduced by a rotation.

We would like to thank the staff of the CSO for their help and support, and particularly Antony Schinckel and Maren Purves, for collecting the $^1H^{12}C^{14}N(4–3)$ data. This work was supported by NSF contract AST 90–15755.

REFERENCES

Bieging, J. H., & Nguyen-Quang-Rieu 1988, ApJ, 324, 516
Burton, M. G., & Geballe, T. R. 1986, MNRAS, 223, 13P
Carsenty, U., & Solf, J. 1982, A&A, 106, 307
Cernicharo, J., Guélin, M., Martín-Pintado, J., Peñalver, J., & Mauersberger, R. 1990, A&A, 222, 1(L)
Crampton, D., Cowley, A. P., & Humphreys, R. M. 1975, ApJ, 198, L135
DeLucia, F., & Gordy, W. 1969, Phys. Rev. 187, 58
Ellison, B. N., & Miller, R. E. 1987, Int. J. Infrared Millimeter Waves, 8, 609
Ellison, B. N., Schaffer, P. L., Schaal, W., Vail, D., & Miller, R. E. 1989, Int. J. Infrared Millimeter Waves, Vol. 10, No. 8
Gammie, C. F., Knapp, G. R., Young, K., Phillips, T. G., & Falgarone, E. 1990, Ap&SS, 345, 87(L)
Heiligman, G. M., et al. 1986, ApJ, 308, 306
Iben, I., & Renzini, A. 1983, ARA&A, 21, 271
Kawabe, R., et al. 1987, 314, 322
Keen, N. J., Mischerikow, K. D., Ediss, G. A., & Perchtold, E. 1986, Electronics Letters, Vol. 22, No. 7, 353
Knapp, G. R. 1986, ApJ, 311, 731
Knapp, G. R., Phillips, T. G., Leighton, R. B., Lo, K. Y., Wannier, P. G., & Wootten, H. A. 1982, ApJ, 252, 616
Kwok, S., & Bignell, R. C. 1984, ApJ, 276, 544
Morris, M. 1980, ApJ, 236, 823
———. 1981, ApJ, 249, 572
Morris, M. 1987, PASP, 99, 1115
Morris, M., & Alcock, C. 1977, ApJ, 218, 687
Morris, M., Lucas, R., & Omont, A. 1985, A&A, 142, 107
Ney, E. P., Merrill, K. M., Beklin, E. E., Neugebauer, G., & Wynn-Williams, C. G. 1975, ApJ, 198, L129
Olofsson, H. 1988, Space Sci. Rev., 47, 145
Press, W. H., Flannery, B. P., Teukolsky, S. A., & Vetterling, W. T. 1988, Numerical Receipes (Cambridge: Cambridge Univ. Press)
Rodríguez, L. F. 1987, in Planetary and Proto–Planetary Nebulae: From *IRAS* to *ISO*, ed. A. P. Martinez (Dordrecht: Reidel), 55
Schönberner, D. 1983, ApJ, 272, 708
Smith, M. G., Geballe, T. R., Sandell, G., & Aspin, C. 1990, in Submillimetre Astronomy, ed. G. D. Watt & A. S. Webster (Dordrecht: Kluwer), 29
Sopka, R. J., Olofsson, H., Johansson, L. E. B., Nguyen-Q-Rieu, & Zuckerman, B. 1989, A&A, 210, 78
Spergel, D. N., Giuliani, J. L., & Knapp, G. R. 1983, ApJ, 275, 330
Truong-Bach, Morris, D., Nguyen-Q-Rieu, & Deguchi, S. 1990, A&A, 230, 431
Wannier, P. G., & Sahai, R. 1987, ApJ, 319, 522
Westbrook, W. E., Becklin, E. E., Merrill, K. M., Neugebauer, G., Schmidt, M., Willner, S. P., & Wynn-Williams, C. G. 1975, ApJ, 202, 407
Yusef-Zadeh, F., Morris, M., & White, R. L. 1984, ApJ, 278, 186